Synchronization scenarios in the Winfree model of coupled oscillators

Rafael Gallego,[1] Ernest Montbrió,[2] and Diego Pazó[3]
[1]*Departamento de Matemáticas, Universidad de Oviedo, Campus de Viesques, 33203 Gijón, Spain*
[2]*Center for Brain and Cognition, Department of Information and Communication Technologies, Universitat Pompeu Fabra, 08018 Barcelona, Spain*
[3]*Instituto de Física de Cantabria (IFCA), CSIC-Universidad de Cantabria, 39005 Santander, Spain*
(Received 24 May 2017; published 17 October 2017)

Fifty years ago Arthur Winfree proposed a deeply influential mean-field model for the collective synchronization of large populations of phase oscillators. Here we provide a detailed analysis of the model for some special, analytically tractable cases. Adopting the thermodynamic limit, we derive an ordinary differential equation that exactly describes the temporal evolution of the macroscopic variables in the Ott-Antonsen invariant manifold. The low-dimensional model is then thoroughly investigated for a variety of pulse types and sinusoidal phase response curves (PRCs). Two structurally different synchronization scenarios are found, which are linked via the mutation of a Bogdanov-Takens point. From our results, we infer a general rule of thumb relating pulse shape and PRC offset with each scenario. Finally, we compare the exact synchronization threshold with the prediction of the averaging approximation given by the Kuramoto-Sakaguchi model. At the leading order, the discrepancy appears to behave as an odd function of the PRC offset.

DOI: 10.1103/PhysRevE.96.042208

I. INTRODUCTION

Macroscopic synchronization is a well-known emergent phenomenon arising in ensembles of oscillators when, despite their unavoidable differences, some fraction of the oscillators spontaneously lock to one another and oscillate together with exactly the same frequency [1–3]. Examples of collective synchronization are abundant and surprisingly diverse, see, e.g., Ref. [4]. They include the synchronous flashing of fireflies [5], circadian [6] and cardiac [7] rhythms, the spontaneous transitions to synchronous stepping [8] and to synchronous clapping [9], or the collective synchronization of chemical oscillators [10], and arrays of optomechanical cells [11], and Josephson junctions [12].

The first successful attempt to model macroscopic synchronization is due to Arthur Winfree. In 1967, Winfree proposed a mathematical model consisting of a large population of globally coupled oscillators. Assuming weak coupling, Winfree postulated the dynamics of the individual oscillators to be well described by a single-phase variable. Interactions are modeled by means of pulses that are emitted by each oscillator and perturb the phase velocity of all the other oscillators. Mathematically, this is expressed through two independent functions: The (infinitesimal) phase response curve (PRC), determining how the phase of an oscillator changes under perturbations, and a function specifying for the shape of the pulses. Numerical simulations in Refs. [13,14] showed that, under suitable conditions, the Winfree model displayed a transition from a totally asynchronous state to collective synchronization, analogously to phase transition in statistical mechanics. Though the Winfree model was later investigated in a few more papers [15–17], the interest soon turned to the simpler and renowned Kuramoto model [2–4,18].

A new boost in the theoretical understanding of phase-oscillator populations models occurred in 2008, when Ott and Antonsen (OA) discovered an exact dimensionality reduction of the (infinite-dimensional) Kuramoto model, called OA ansatz [19–21]. The discovery of the OA ansatz opened up the possibility of tackling unresolved problems and investigate novel variants and extensions of the Kuramoto model, see, e.g., Refs. [22–41]. Remarkably, the OA ansatz is also applicable to pulse-coupled oscillators [42–49] and, in particular, to the original Winfree model [50]. This allows to investigate synchronization phenomena which are not accessible using Kuramoto-like models. Specifically, the advantage of the Winfree model is that permits to investigate separately how pulse shape and PRC type influence collective synchronization. Note that the PRC of cells, such as neurons [51,52] and cardiac cells [53], can be measured experimentally. Therefore, understanding better the Winfree model should contribute to narrow the gap between mathematical models and biological phenomena.

Here we build on our previous work [50] and systematically analyze the impact of (i) pulse shapes and (ii) PRC offsets, onto collective synchronization in the Winfree model. We find that the phase diagram obtained in Ref. [50] is not unique and that a novel synchronization scenario emerges for certain pulse types via the mutation of a codimension-two Bogdanov-Takens (BT) point. We end investigating the limit in which the oscillators are nearly identical and very weakly coupled. In that situation, the averaging approximation is valid, and a Kuramoto-like model captures the dynamics with a level of accuracy that is measured numerically.

The paper is organized as follows: In Sec. II we introduce the Winfree model and discuss the pulses and PRC types under investigation. In Sec. III, we consider the thermodynamic limit of the Winfree model and derive two ordinary differential equations (ODEs) that exactly describe the temporal evolution of the complex Kuramoto order parameter in the Ott-Antonsen invariant manifold. In Sec. IV, we present the results obtained from those two ODEs, for a variety of pulse shapes and PRCs, and check the validity of the results with simulations of a finite population of Winfree oscillators. In Sec. V, we compare the Winfree model with its averaging approximation. Finally, in Sec. VI, we address the conclusions of this work.

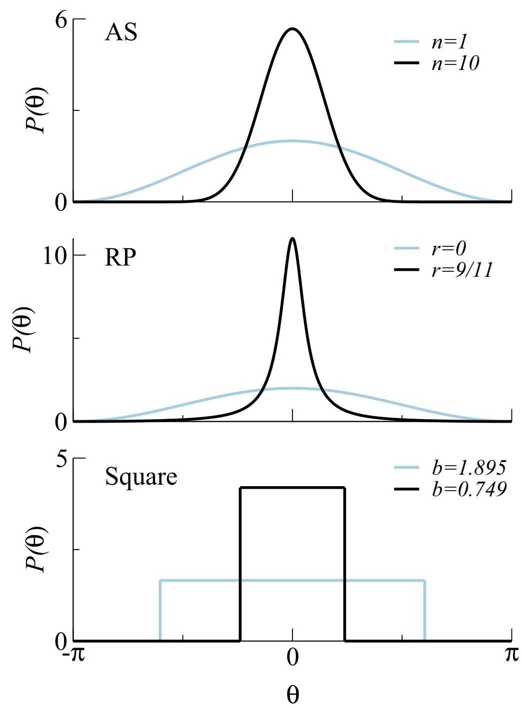

FIG. 1. AS, Ariaratnam-Strogatz; RP, rectified-Poisson, and Square pulse functions $P(\theta)$, for two different widths. Functions of the same color have the same shape factor Π; see Eq. (16). See also Table I for the detailed mathematical form of the pulses and shape factors.

II. THE WINFREE MODEL

The Winfree model consists of an ensemble of $N \gg 1$ globally coupled phase oscillators with heterogeneous natural frequencies ω_i, $i = 1,\ldots,N$ [13,14]. The phases θ_i are governed by the set of N ordinary differential equations (ODEs):

$$\dot{\theta}_i = \omega_i + Q(\theta_i)\,\frac{\varepsilon}{N}\sum_{j=1}^{N} P(\theta_j). \tag{1}$$

All the oscillators receive the same inputs via the mean field $h = N^{-1}\sum_{j=1}^{N} P(\theta_j)$. Their response to the mean field depends on the state of each oscillator θ_i and is determined by the PRC function $Q(\theta)$. Both P and Q are 2π-periodic functions on the real line and hence can be defined either in the range $[0,2\pi)$ or in the range $[-\pi,\pi)$. Finally, the global coupling strength is controlled by the parameter $\varepsilon > 0$.

A. Pulse shape, $P(\theta)$

The function P in Eq. (1) specifies the form of the pulses. We only consider pulses with the following properties:

(i) P is unimodal and symmetric around $\theta = 0$.

(ii) P vanishes at $\theta = \pi$.

(iii) P has a normalized area: $\int_{-\pi}^{\pi} P(\theta)d\theta = 2\pi$.

We consider the three pulse types with finite width shown in Fig. 1 and defined in Table I. The first pulse, labeled as AS, was originally adopted by Ariaratnam and Strogatz [15] and is commonly used in recent studies of pulse coupled-phase oscillators [42–45,48–50,54]. Additionally, we consider a variant of the pulse used by O'Keeffe and Strogatz in Ref. [48] equal to the Poisson kernel but with an offset so that it fulfills the condition (ii). We term this pulse as "rectified Poisson kernel" (RP). Finally, we consider a square pulse with a flat profile and vanishing in a finite interval of θ: $[-\pi,-b)\cup(b,\pi)$.

Concerning the macroscopic dynamics of the Winfree model, the precise value of N becomes irrelevant provided it is large enough (i.e., only trivial finite-size fluctuations are observed; see below). However, for Dirac δ pulses, this is not the case, as we discuss in Sec. IV D. The Dirac δ is the limiting case of the pulse types considered, i.e., $n \to \infty$, $r \to 1$, and $b \to 0$ for the AS, RP, and square pulses, respectively.

B. Phase-response curve (PRC), $Q(\theta)$

The influence of a certain (small) perturbation on the phase of an oscillator is determined by the PRC, $Q(\theta)$. Here, we assume that (i) the PRC vanishes at the phase where the pulses peak, i.e., at $Q(\theta = 0) = 0$; and (ii) the PRC has a sinusoidal shape. This latter condition is crucial, for the OA theory to be applicable. The constraints (i) and (ii) lead us to the following one-parameter family of PRCs:

$$Q(\theta) = \frac{\sin\beta - \sin(\theta+\beta)}{\cos\beta} = q(1-\cos\theta) - \sin\theta, \tag{2}$$

where parameter $q = \tan\beta$ determines the degree of asymmetry of the PRC. As illustrated in Fig. 2, Q is more positive (advancing) than negative for $q > 0$, while it is more negative (retarding) for $q < 0$. The case $q = 0$ corresponds to a perfectly balanced PRC. Hence, we call q "offset parameter" hereafter. Note that in Ref. [50] the PRC is defined in a slightly different manner: Here, ε is equivalent to $\varepsilon\cos\beta$ in our previous work.

C. Frequency distribution, $g(\omega)$

As indicated above, heterogeneity in the population enters through the set of natural frequencies ω_i. As we show in the next section, to simplify the analysis of the Winfree model Eq. (1), it is convenient to adopt a Lorentzian distribution centered at ω_0 with half-width Δ:

$$g(\omega) = \frac{\Delta/\pi}{(\omega-\omega_0)^2 + \Delta^2}. \tag{3}$$

III. DIMENSIONALITY REDUCTION

We turn now to the analysis, and apply the so-called Ott-Antonsen theory to derive a low-dimensional system of ODEs that, under some assumptions specified below, determines the mean-field, long-term dynamics of the Winfree model in the thermodynamic limit $N \to \infty$ [55]. Hence, we introduce a density function F, such that $F(\theta|\omega,t)\,d\theta$ represents the fraction of oscillators with phases between θ and $\theta + d\theta$ and natural frequency ω at a time t. The density F satisfies the continuity equation,

$$\partial_t F + \partial_\theta(F\dot{\theta}) = 0, \tag{4}$$

TABLE I. Summary of the various pulse functions considered. The normalizing constant of the AS pulse is $a_n = 2^n(n!)^2/(2n)! = n!/(2n-1)!!$. The fourth column shows the mean field $h(Z)$, which is the function entering in Eq. (11) describing the system's mean-field dynamics exactly. In the last column, the shape factor Π quantifies the effective strength of each pulse under the averaging approximation; see Eq. (16). In Fig. 1, lines of the same style share the same Π value.

Pulse name	$P(\theta)$	Parameter	Mean field: $h(Z)$	Shape factor: Π
Ariaratnam-Strogatz (AS)	$a_n(1+\cos\theta)^n$	$n \in \mathbb{Z}^+$	$1+(n!)^2\sum_{k=1}^{n}\frac{Z^k+(Z^*)^k}{(n+k)!(n-k)!}$	$\frac{n}{n+1}$
Rectified-Poisson (RP)	$\frac{(1-r)(1+\cos\theta)}{1-2r\cos\theta+r^2}$	$r \in (-1,1)$	$\mathrm{Re}[\frac{1+Z}{1-rZ}]$	$\frac{1+r}{2}$
Square	$\begin{cases}\pi/b \text{ for } \lvert\theta\rvert \leqslant b\\ 0 \text{ otherwise}\end{cases}$	$b \in (0,\pi)$	$1-\frac{1}{b}\mathrm{Im}[\ln(1-Ze^{ib})-\ln(1-Ze^{-ib})]$	$\frac{\sin b}{b}$
Dirac δ	$2\pi\delta(\theta)$	—	$\mathrm{Re}[\frac{1+Z}{1-Z}]$	1

and, since it is 2π-periodic in θ, it admits the Fourier expansion,

$$F(\theta|\omega,t) = \frac{1}{2\pi}\left\{1+\left[\sum_{m=1}^{\infty}\alpha_m(\omega,t)e^{im\theta}+\text{c.c.}\right]\right\}, \quad (5)$$

where c.c. denotes complex conjugation.

The Winfree model belongs to the class of phase oscillator systems,

$$\dot{\theta}_i(t) = \omega_i + B(t) + \mathrm{Im}[H(t)e^{-i\theta_i(t)}], \quad (6)$$

with the particular form of the common forcing terms $B(t) = q\varepsilon h(t)$ and $H(t) = \varepsilon(1-iq)h(t)$. In the thermodynamic limit, systems of the general form of Eq. (6) admit solutions F in the so-called Ott-Antonsen (OA) manifold [19],

$$F(\theta|\omega,t) = \frac{1}{2\pi}\left\{1+\left[\sum_{m=1}^{\infty}[\alpha(\omega,t)]^m e^{im\theta}+\text{c.c.}\right]\right\}, \quad (7)$$

which is simply Eq. (5) with the coefficients $\alpha_m(\omega,t) = [\alpha(\omega,t)]^m$; see, e.g., Refs. [20,21,35,50,56]. Furthermore, in Refs. [20,21] it was also shown that, for analytic frequency distributions $g(\omega)$, the OA manifold is the unique attractor and hence, if F does not initially satisfy Eq. (7), it subsequently converges (in the sense of Refs. [20,21]) to it [57]–although in some cases the convergence can be very slow [58]. In the following, we restrict our attention to the OA manifold Eq. (7) where the system can be easily analyzed.

Substituting the OA ansatz Eq. (7) into the continuity Eq. (4), we find

$$\partial_t\alpha = -i(\omega+\varepsilon hq)\alpha + \frac{\varepsilon h}{2}[(1+iq)-(1-iq)\alpha^2], \quad (8)$$

where the mean field,

$$h(t) = \int_{-\infty}^{\infty} g(\omega)\int_0^{2\pi} F(\theta|\omega,t)\,P(\theta)\,d\theta\,d\omega, \quad (9)$$

couples every $\alpha(\omega,t)$ with all others $\alpha(\omega',t)$.

The complex Kuramoto order parameter Z quantifies the amplitude of first Fourier mode of the density F and reads

$$Z(t) = \int_{-\infty}^{\infty} g(\omega)\int_0^{2\pi} F(\theta,\omega,t)e^{i\theta}\,d\theta\,d\omega.$$

Under the assumption that the system evolves in the OA manifold the previous equation writes

$$Z^*(t) = \int_{-\infty}^{\infty} g(\omega)\,\alpha(\omega,t)\,d\omega,$$

where the asterisk denotes complex conjugation. For Lorentzian $g(\omega)$, this integral over the real line can be computed by performing an analytical continuation of $\alpha(\omega,t)$ from real ω into complex $\omega = \omega_r + i\omega_i$; see Ref. [19] for details. Closing the integral by a half-circle at infinity in the lower complex ω half-plane permits us to apply the residue theorem, which gives

$$Z^*(t) = \alpha(\omega_p,t), \quad (10)$$

where $\omega_p = \omega_0 - i\Delta$ is the simple pole of $g(\omega)$ inside the integration contour. Then, setting $\omega = \omega_p$ in Eq. (8), we obtain

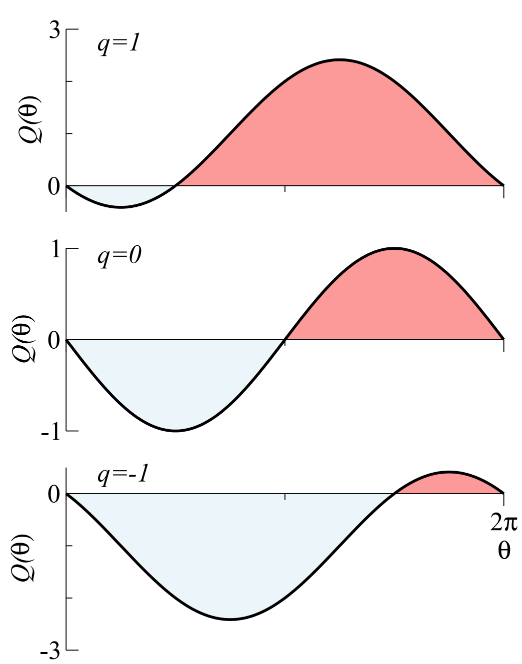

FIG. 2. Phase-response curves [Eq. (2)] for $q = 1,0,-1$. Brief, perturbations lead to either a phase delay (light-shaded blue) or a phase advance (shaded red), depending on the phase θ of the oscillator. The sign and magnitude of parameter q controls the offset of the PRC and hence determines if pulse interactions are mostly promoting ($q > 0$) or delaying ($q < 0$) phase shifts.

the complex-valued ODE,

$$\dot{Z} = (-\Delta + i\omega_0)\, Z + \frac{\varepsilon h}{2}[1 - Z^2 - iq\,(1 - Z)^2], \quad (11)$$

for the complex Kuramoto order parameter Z. To close Eq. (11), one needs to express the mean-field as $h(Z)$. With that aim, it is convenient to expand P in Fourier series:

$$P(\theta) = \sum_{m=-\infty}^{\infty} c_m e^{im\theta}, \quad (12)$$

with $c_m = c_{-m} \in \mathbb{R}$ and $c_0 = 1$, because of the properties (i) and (iii) stipulated in Sec. II A. Inserting Eqs. (12) and (5) into Eq. (9), we get

$$h = 1 + \sum_{k=1}^{\infty} c_k \int_{-\infty}^{\infty} g(\omega)\{[\alpha(\omega,t)^*]^k + [\alpha(\omega,t)]^k\} d\omega, \quad (13)$$

which again can be simplified applying the residues theorem, and recalling that Eq. (10) allows us to express the result in terms of Z only,

$$h = 1 + \sum_{k=1}^{\infty} c_k [Z^k + (Z^*)^k]. \quad (14)$$

This relation permits us to achieve, after some algebra, the desired expressions of $h(Z)$ for the set of pulse types. They are listed in the fourth column of Table I.

Note that, compared to the AS pulse used in previous studies [15,42–45,48–50,54], the RP pulse has the advantage that $h(Z)$ remains a simple function of Z, no matter how much the pulse width is decreased; see Table I. Moreover, though the mean-field function $h(Z)$ for square pulses is more cumbersome than that of the RP pulses, it still permits us to investigate Eq. (11) with pulses of arbitrary small width, without the drawback of dealing with the long sums of the AS pulse's mean field.

IV. PHASE DIAGRAMS AND PHASE PORTRAITS

In this section, we analyze the attractors and bifurcations of the ODEs Eq. (11) for particular instances of the PRC offset q and the pulse type $P(\theta)$. The dynamics of Eq. (11) depends on five parameters: the coupling strength (ε), the pulse width (through n, r or b), the center and half-width of the frequency distribution (ω_0 and Δ), and the PRC offset (q). From now on, and without lack of generality, we set $\omega_0 = 1$, since this can always be achieved after a trivial rescaling of time and parameter ε. In the following, using the MATCONT toolbox of MATLAB, we identify and continue the bifurcations of Eq. (11) in the (ε,Δ) parameter space for the pulse functions described in Table I and for various PRC offsets q.

A. Rectified-Poisson (RP) pulse

Figure 3 shows the phase diagram for the RP pulse ($r = 0.5$) with negative PRC offset ($q = -1$). The diagram is qualitatively identical to those presented in Ref. [50] for the AS pulse, indicating certain robustness of the dynamics against modifications of the pulse shape. In Fig. 4(a), we show a sketch of the phase portraits in the regions of interest. In the shaded region, labeled 2, Eq. (11) has one attractor of limit-cycle type, meaning that Z exhibits periodic oscillations.

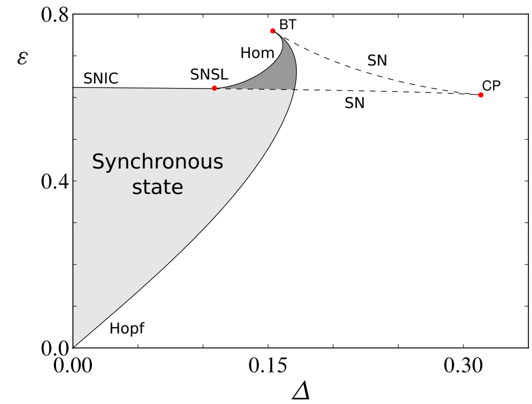

FIG. 3. Phase diagram of the Winfree model in the (Δ,ε)-plane for a PRC with $q = -1$ and a RP pulse with $r = 0.5$. Bifurcation lines are obtained from Eq. (11). In the shaded region there is a stable limit-cycle corresponding to a macroscopic synchronized state; see Fig. 5(c). The boundary of synchronization are Hopf, SNIC, and homoclinic bifurcation lines. In the dark shaded region the limit cycle (synchronization) coexists with a stable fixed point (asynchronous state). Accordingly the dashed lines are the loci saddle-node bifurcations. Finally, note that three codimension-two points organize the bifurcation lines: double-zero eigenvalue Bogdanov-Takens (BT), cusp (CP), and saddle-node separatrix-loop (SNSL).

This is reflecting a state of macroscopic synchronization in which a certain part of the population is self-entrained to a common frequency. There are three different paths leading to this macroscopic state, depending on which bifurcation line is crossed: Hopf, SNIC (saddle-node on the invariant circle), or Hom (homoclinic or saddle-loop). Note that the latter one is a global bifurcation that does not destabilize the macroscopic steady state, and in consequence, a region of bistability between synchrony and asynchrony exists; see the dark shaded region in Figs. 3 and 4(a). Two lines of saddle-node bifurcations of fixed points, emanating from a cusp point (CP), complete the phase diagram and bound a region of bistability between two stable equilibrium points (region 4). They correspond to two macroscopic asynchronous states with a different proportion of quiescent oscillators. For large enough Δ, namely above the CP point, the fraction of quiescent oscillators varies smoothly (i.e., nonhysteretically) with ε.

Next, we numerically compare the dynamics of the reduced model Eq. (11) with that of a finite population of $N = 2000$ Winfree oscillators. In Figs. 5(a) and 5(c), we present raster plots corresponding to macroscopic asynchronous and synchronized states, respectively (a dot is plotted every time an oscillator crosses a multiple of 2π). In Figs. 5(b) and 5(d), we display the dynamics of $Z = N^{-1}\sum_j e^{i\theta_j}$ with solid lines, and compare with the results from Eq. (11) in red. The agreement is very good up to finite-size fluctuations.

Moreover, to be more systematic we swept parameter ε along $\Delta = 0.15$, i.e., a vertical line in Fig. 3, with the intention of testing that the bifurcations were indeed reproduced. As the rotation of the oscillators is not uniform, $|Z|$ is not a useful order parameter to characterize the synchronization transition since it never vanishes. In the thermodynamic limit, we have $|Z| = \text{const.}$ in the macroscopic asynchronous state and time-

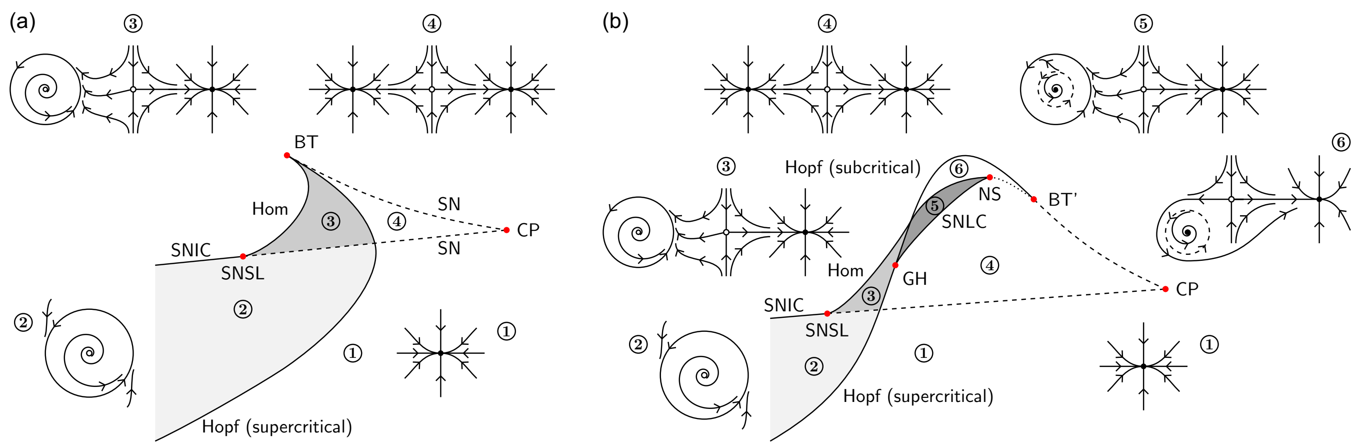

FIG. 4. Possible synchronization scenarios of the Winfree model Eq. (1). Panels (a) and (b) are sketches of the phase diagrams and phase portraits in the different regions of the (Δ,ϵ)-plane. Graph (a) displays a typical diagram when a BT point comes into play [50], whereas graph (b) corresponds to the case of a BT′ point (see text for more details). Some details such as the transition from stable node to stable focus or the annihilation of saddle and unstable node have been omitted for simplicity.

periodic $|Z|$ in the macroscopic synchronous state. It is more convenient to use the order parameter proposed by Shinomoto and Kuramoto [60],

$$\zeta = \overline{|Z - \overline{Z}|}, \tag{15}$$

where the bars denote long-time average. For asynchronous dynamics, the Shinomoto-Kuramoto order parameter Eq. (15) satisfies $\zeta = 0$, while $\zeta \neq 0$ indicates some degree of synchronization. Figure 5(e) shows that the results of our numerical simulations of the original Winfree model show a good agreement with the reduced ODE, Eq. (11). Below the Hopf bifurcation and above the homoclinic one, ζ is not exactly zero due to the finiteness of the population; indeed, $\zeta \sim O(N^{-1/2})$ in both regions. At large ε the comparatively smaller finite-size fluctuations can be attributed to the fact that most oscillators are in a macroscopic quiescent state with basically no contribution to the fluctuations.

We next investigate how the synchronization region changes as the pulse width varies. Figures 6(a) and 6(b) show the synchronization boundaries for $r = 0$, 0.5, and 0.95, and opposite values of the PRC's offset q $(= \mp 1)$. For the sake of clarity other bifurcation lines have been omitted. For positive offsets, we find the same result that we found in Ref. [50] for AS pulses with highly unbalanced PRCs ($q \gg 0$): Narrow RP pulses (r close to 1) are more efficient than broad pulses to synchronize heterogeneous populations of oscillators. Indeed, note that the synchronization boundary of the narrowest pulse ($r = 0.95$) reaches the highest value of the heterogeneity parameter Δ in Fig. 6(b). However, a small discrepancy with this previous rule was already noticeable in the $q = 0$ curve of Fig. 2(a) in Ref. [50]. Here we revisit that question and find that, as Fig. 6(a) shows, for negative PRC offsets the discrepancy is even more dramatic: the Hopf boundary is far from attaining the largest Δ value for the narrowest pulse. Hence, synchronization is not optimal for narrow pulses, but it also depends on the sign of the PRC's offset q. Consequently, one is tempted to wonder if, in nature, adaptation may in some cases drive PRC offsets and pulse widths to be mutually optimized in a certain sense.

B. Ariaratnam-Strogatz (AS) pulse

Thus far we found no qualitative difference between the phase diagram for RP pulses of Fig. 3, with that of Ref. [50], obtained using AS pulses. Nonetheless, in this section we show that this qualitative agreement breaks down for AS pulses with PRCs with negative offset.

The AS pulse with $n = 1$ is identical to the RP pulse with $r = 0$, so that no differences arise in this case. Surprisingly, when we considered narrower pulses (larger values of n) a more complicated bifurcation scenario showed up; see Fig. 7 for $n = 5$ and $q = -1$. Indeed, at a certain critical n, the Bogdanov-Takens point mutates its character in such a way that the Hopf line emanating from it becomes of subcritical type, while the homoclinic bifurcation now involves an unstable periodic orbit—because the sum of the eigenvalues of the saddle point, called saddle quantity, is positive. This mutated Bogdanov-Takens point is designated as BT′ hereafter. Points BT and BT′ are both equally generic double-zero-eigenvalue points consistent with the normal form in textbooks [61,62]: BT is the usual representation (up to a transformation of parameters), while BT′ is also consistent upon time inversion.

In the transition from BT to BT′ two new codimension-two points appear:

(1) A generalized Hopf (GH) point on top of the Hopf line where the bifurcation shifts from super- to subcritical.

(2) A neutral saddle (NS) point where the homoclinic connection is degenerate, since it involves a saddle point with zero saddle quantity [62]. At the NS point the line of homoclinic bifurcation of the *stable* limit cycle terminates.

The GH and NS points are connected by a new line, which is the locus of a saddle-node bifurcation of limit cycles (SNLC). Figure 4(b) shows sketches of the phase portraits when a BT′ point is present in the phase diagram. Notably, the synchronization region is detached from the BT′ point, and a region with three attractors (i.e., *tristability*) exists. This

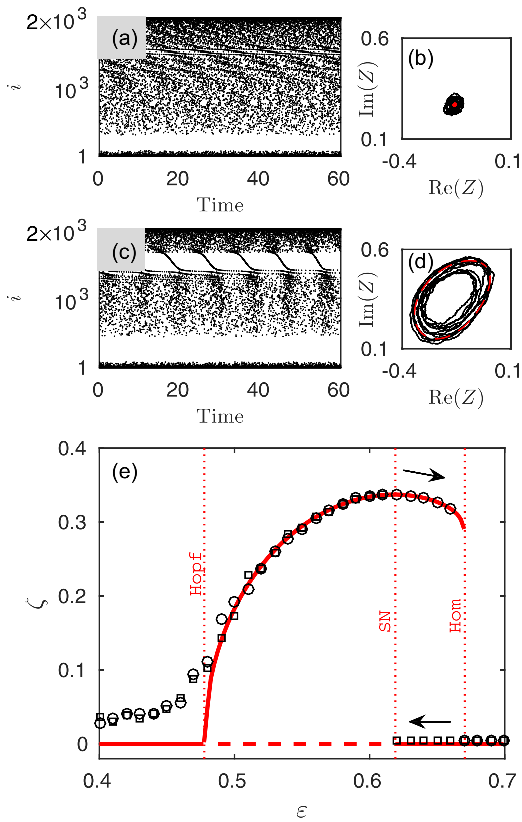

FIG. 5. (a) Raster plot for a system of $N = 2000$ "Winfree oscillators" with $q = -1$ and RP pulses with $r = 0.5$—as in Fig. 3—with a coupling strength $\varepsilon = 0.4$. The natural frequencies have been deterministically selected from a Lorentzian distribution with $\omega_0 = 1$ and $\Delta = 0.15$, using $\omega_i = \omega_0 + \Delta \tan[\pi(2i - N - 1)/(2N)]$. The horizontal white stripe corresponds to oscillators with natural frequencies near zero that remain quiescent. (b) Phase portrait of the macroscopic state in panel (a) is depicted with a solid line, and the stable fixed point of Eq. (11) is depicted as a red point. Panels (c) and (d) are equivalent to (a) and (b), but with $\varepsilon = 0.5$. For this parameter value the system displays a certain degree of synchrony. Note that in panel (d), Eq. (11) exhibits a stable limit cycle represented as a red dashed line. (e) Bifurcation diagram ζ vs. ε along the line $\Delta = 0.15$. The red lines are obtained from the low-dimensional Eq. (11), and the bifurcations (Hopf, saddle-node, and homoclinic, from left to right) are marked by vertical dotted lines. Symbols correspond to numerical simulations of the Winfree model. Circles (respectively, squares) are obtained by increasing (respectively, decreasing) ε in steps of magnitude 0.01. The simulations were initiated with the oscillator phases randomly chosen from the interval $[-\pi,\pi)$, followed by a transient of 1000 t.u. The time-averaged quantities $\overline{Z}$ and ζ are computed sequentially for time intervals of 1000 t.u. each. The numerical integration of the population was carried out with a fifth-order Runge-Kutta scheme with adaptive stepsize control [59].

region is the approximate triangle with vertices at GH and NS visible both in the inset of Fig. 7 and in Fig. 4(b), region 5. There, the limit cycle (corresponding to synchronization) coexist with two stable fixed points. Note that by entering into region 5 through the saddle-node bifurcation of limit cycles line (connecting the points GH and NS) a finite-sized limit cycle with a finite basin of attraction suddenly appears.

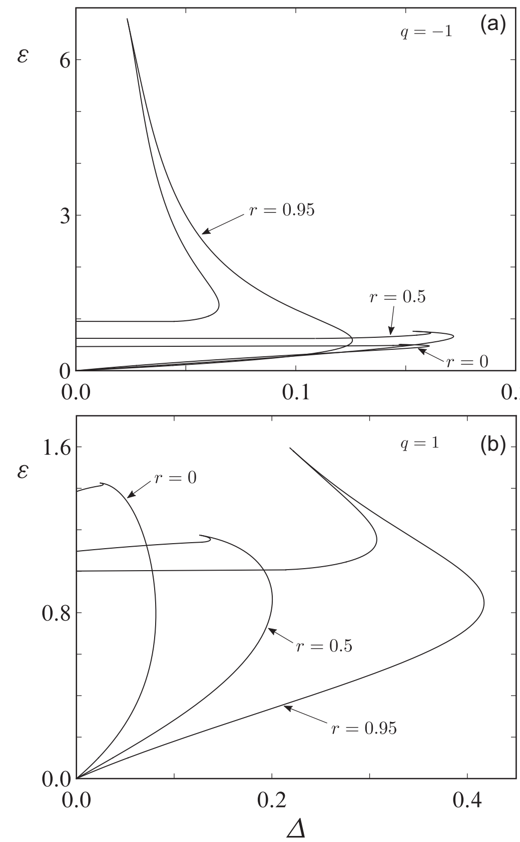

FIG. 6. Boundaries of the synchronization region in the (Δ,ε)-plane for the RP pulse and several values of r. Graphs (a) and (b) correspond to $q = -1$ and $q = 1$, respectively.

C. Transition between the synchronization scenarios BT and BT′

In view of the distinct phase diagrams associated to BT and BT′, next we investigate the conditions under which each scenario shows up. Our systematic numerical investigation indicates that the RP pulse is always associated to a BT point.

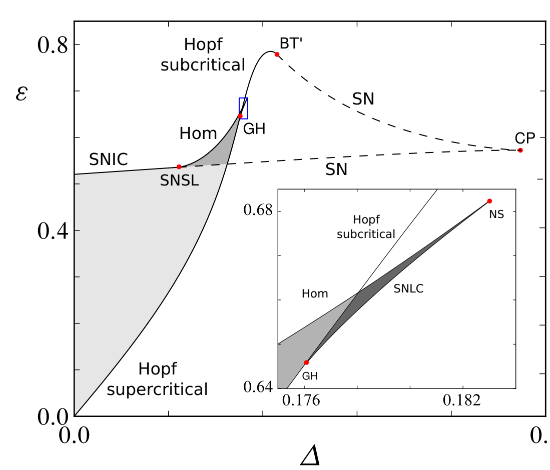

FIG. 7. Phase diagram of the Winfree model in the (Δ,ε)-plane for the AS pulse. Parameter values are $q = -1$ and $n = 5$; the inset is a zoom of the region enclosed by a rectangle in the main plot.

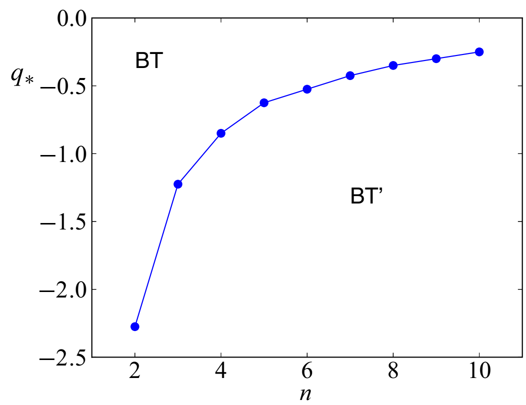

FIG. 8. Numerically obtained critical boundary q_* separating the regions BT and BT′, as a function of the AS pulse width n. The novel synchronization scenario, associated to a BT′ point, shows up for narrow pulses and negative PRC offsets.

In the case of the AS pulse, we determined numerically the threshold value of q, which we designated as q_*, where the transition between BT and BT′ occurs, i.e. the q value at which a degenerate (codimension-three) BT point arises. The result covering all integer values $n \leqslant 10$ is depicted in Fig. 8 and demonstrates that the BT′ point only arises for sufficiently negative offsets q. Noteworthy, when n grows, BT′ can be observed for increasing small values of $|q|$. The absence of a point for $n = 1$ in Fig. 8 is not an omission; in fact, we failed to numerically find a BT′ point even after considering extremely small values of q—recall also that the AS pulse with $n = 1$ coincides with the RP pulse with $r = 0$. Finally, we carried out numerical simulations using square pulses (not shown), and found that the bifurcation scenario associated to BT′ is observed already for $q = 0$, provided that b is smaller than $b_*(q = 0) = 1.02\ldots$ (a significantly large value).

To get some more physical insight, we examined the asymptotic behavior of $P(\theta)$ in a neighborhood of $\theta = \pi$ for each pulse type. They are

$$P(\pi \pm \delta\theta) \simeq \frac{1-r}{2(1+r)^2}\delta\theta^2, \frac{(n!)^2}{(2n)!}\delta\theta^{2n}, 0,$$

for RP, AS, and square pulses, respectively. The marked differences of the respective asymptotics led us to conjecture a simple rule of the thumb: pulses that fall fast enough to zero at $\theta = \pi$ are prone to exhibit the synchronization scenario with five codimension-two points, i.e., BT′. On the contrary, pulses that fall to zero more slowly (such as the RP pulse) favor the first scenario (BT), making the second scenario (BT′) impossible or only present for small enough PRC offsets q.

D. Dirac δ pulse

All the pulses studied in this paper have the Dirac δ as limiting case. It is not difficult to obtain the expression of $h(Z)$ for the Dirac δ pulse; see Table I. Nonetheless, some caution must be taken here: for obtaining the mean field $h(Z)$ the thermodynamic limit ($N \to \infty$) is assumed prior to the zero width pulse limit, and it is well known that these two limits do not commute [63]. Therefore, the results we obtain for Dirac δ pulses cannot be exactly reproduced in numerical simulations, which necessarily involve a finite number of oscillators. Accordingly, the results obtained here for Dirac δ pulses must be interpreted as a limit of the bifurcation lines for very narrow pulses. This allows us to put aside the pulse shape and to focus solely on the influence of the PRC offset parameter q.

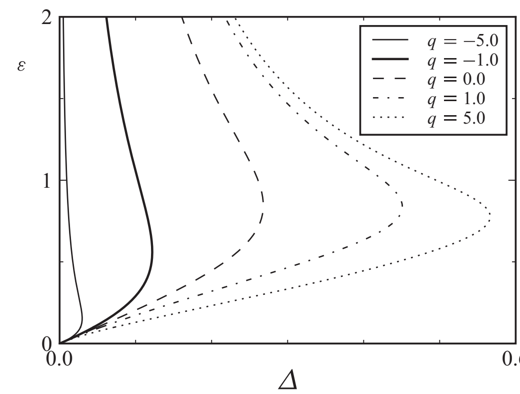

FIG. 9. Phase diagram of the Winfree model in the (Δ,ε) plane for the Dirac δ pulse and several values of q.

Figure 9 shows phase diagrams in the (Δ,ε) plane for Dirac δ pulses and for several values of q. The curves displayed are Hopf bifurcation lines that emanate from the origin and approach the vertical axis when $\varepsilon \to \infty$. As mentioned above, there are subtle questions regarding this pulse, so the Hopf bifurcation lines have to be understood simply as the limit of the Hopf curves for very narrow pulses. In fact, the absence of the saddle-node bifurcations lines indicates a certainly singular behavior in that limit.

Yet, from Fig. 9, we can conclude that the synchronization region increases monotonically with q. Our physical interpretation of this feature is that, for negative PRC offsets, the bias of the PRC tends to slow down the oscillators favoring the formation of a cluster with quiescent oscillators (partial oscillation death). On the contrary, positive PRC offsets generally favor phase advances, retarding the accumulation of quiescent oscillators and leaving room for the synchronization to occur more widely.

Let us finally point out that the bifurcation lines can be analytically obtained by transforming Eq. (11) into a complex-valued ODE for a new variable $w = (1+Z)/(1-Z)$, such that $h = \mathrm{Re}(w)$. In the new coordinate system, and with the assistance of MATHEMATICA, we derived convoluted but nonetheless exact equations of the Hopf boundaries in parametric form:

$$\Delta_H(y) = \frac{f(y,q)[-g(y,q) + y(q+y) + 1]}{(y^2+1)(2q+y)},$$

$$\varepsilon_H(y) = \frac{2f(y,q)\{g(y,q)(y^2-1) + y[q(y^2+3) + y] + 1\}}{(y^2+1)(2q+y)(4qy - y^2 + 3)},$$

with

$$g(y,q) \equiv \sqrt{(q^2+1)y^2+1},$$
$$f(y,q) \equiv \sqrt{2g(y,q) + 2qy - y^2 - 1},$$

where $y \in (0,\infty)$. In passing, we note that for $q = 0$, a simple explicit formula can be found; see Ref. [36] in Ref. [50].

V. LIMIT OF WEAK COUPLING AND NEARLY IDENTICAL OSCILLATORS

To conclude, we investigate the Winfree model in the limit of weak coupling and weak heterogeneity, i.e., $|\varepsilon| \ll 1$, $\Delta \ll 1$. This is an important limiting case, since the method of averaging can be applied and the Winfree model reduces to the well-studied Kuramoto-Sakaguchi (KS) model [64,65]. Our aim in this section is to investigate how the synchronization threshold of the Winfree model deviates from that of its corresponding KS model, for different pulse functions and PRC types.

A. Averaging approximation: Kuramoto-Sakaguchi model

In the classical analysis by Kuramoto [64], weakly interacting oscillators with frequencies close to a resonance are described by means of the averaging approximation. In the case of 1:1 resonance (nearly identical frequencies), the interaction term between any two oscillators becomes a function of their phase difference.

Given that the PRCs considered here are chosen to be sine-shaped, the only resonant term is the first harmonic. Thus, the averaging calculation leads to the KS model [50,64,65]:

$$\dot{\theta}_i = \omega_i + \varepsilon q + \Pi \frac{\varepsilon}{N} \sum_{j=1}^{N} [\sin(\theta_j - \theta_i) - q\cos(\theta_j - \theta_i)]. \tag{16}$$

The parameter Π is a "shape factor" that depends on the pulse shape. The shape factor depends only on the first harmonic of the pulse, or more precisely, $\Pi = c_1$; see Eq. (12). The dependence of Π on the parameter controlling the pulse width can be found in the last column of Table I. In all cases, the effective interaction strength increases as the pulses become narrower. In fact, the largest Π value is attained for the Dirac δ pulse.

Generally, for unimodal frequency distributions, the KS model Eq. (16) displays a simple transition between a macroscopic asynchronous, incoherent state ($Z = 0$ in the thermodynamic limit) and macroscopic synchronization at a critical finite value of ε —but see Refs. [36,66] for exceptions. The synchronous state is characterized by the appearance of a subset of oscillators that rotate with a common frequency and have their phases locked, thanks to the mutual coupling that is able to overcome the disparity of the natural frequencies. For the Lorentzian distribution of frequencies, Eq. (3), the critical coupling of the synchronization transition in the thermodynamic limit ($N \to \infty$) can be obtained analytically [65]:

$$\varepsilon_c^{(\mathrm{av})} = \frac{2\Delta}{\Pi}, \tag{17}$$

where the superscript "(av)" is used to emphasize that this is the critical coupling of the averaged model in Eq. (16). Curiously, within this approximation ε_c does not depend on q. (This has to be attributed to the special properties of the Lorentzian distribution $g(\omega)$, which usually yields particularly simple results in Kuramoto-like models.) The exact critical coupling of the Winfree model is computed numerically below and, as presumed, depends on q.

B. Synchronization threshold: Winfree versus KS model

To test the goodness of the averaging approximation, we next compare the synchronization threshold of the Winfree model with the threshold of its averaged counterpart, given by Eq. (17). Our aim is to determine if certain pulses deviate more from the averaging approximation and whether these results depend on the PRC offset q. To make the comparison significant we considered different pulse types with the same Π values. In different panels of Fig. 1, pulses plotted with the same line style have identical shape factor Π, and therefore they yield the identical KS model upon averaging. In turn, the prediction of Eq. (17) is exactly the same for all pulse types (provided the same Π value). To measure the deviation of the Winfree model from the the KS model, we define the quantity

$$\rho(\Delta) = \frac{\varepsilon_H - \varepsilon_c^{(\mathrm{av})}}{\varepsilon_c^{(\mathrm{av})}}, \tag{18}$$

which is proportional to the difference between the exact and the approximated critical couplings (normalized by the approximated critical coupling). For each pulse type and q value, the locus of the Hopf bifurcation $\varepsilon_H(\Delta)$ is numerically available from the exact low-dimensional Eq. (11).

In Fig. 10, we graph ρ for $\Pi = 10/11$ and the three pulse types considered, adopting three values $q = -1$, 0, and 1 in Figs. 10(a), 10(b) and 10(c), respectively. As expected $\rho(\Delta \to 0) = 0$, indicating the validity of the averaging approximation in this limit. As Δ is increased from zero, $\rho(\Delta)$ becomes positive for $q = -1$ and negative for $q = 1$, which implies that synchronization is hindered (promoted) with respect to the averaging approximation for negative (positive) q. (This is also consistent with Fig. 9.) Numerical evidence shows that

$$\rho(\Delta) = \xi(q)\Delta + O(\Delta^2),$$

where $\xi(q)$ is a pulse-dependent odd function (and possibly monotonically decreasing). Note that this means that the best pulse type, in a certain sense, for $q > 0$, becomes the worst for $q < 0$. For instance, for $q = -1$, synchronizability is the best for the square pulse among the pulses considered, but this becomes just the opposite for $q = 1$. The case $q = 0$ is the boundary between these scenarios, because $\xi(0) = 0$. Accordingly, the inset of Fig. 10(b) confirms a nonlinear dependence, namely quadratic, of $\rho(\Delta \ll 1)$.

VI. CONCLUSIONS

The Winfree model critically influenced the development of the theory of synchronization, but it has been scarcely studied in detail due to its mathematical complexity, compared to the Kuramoto model. Nevertheless, the Winfree model permits us to investigate synchronization phenomena beyond the usual assumptions of weak coupling and low-frequency heterogeneity, implicitly assumed in the abundant literature investigating Kuramoto-like models. The recent discovery that the so-called OA theory [19–21] can also be applied to the Winfree model with sinusoidal PRC [50] allows for the

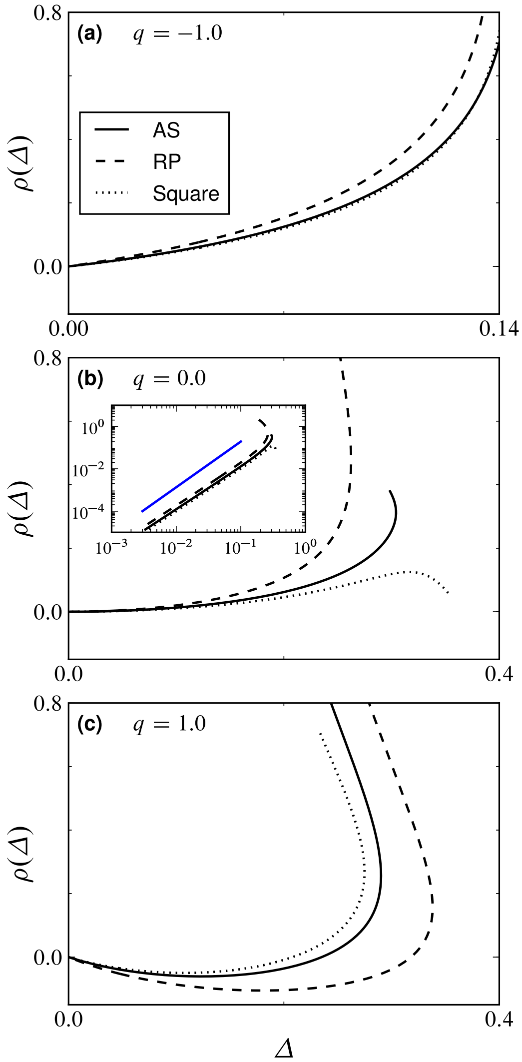

FIG. 10. Quantity $\rho(\Delta)$, Eq. (18), measuring the deviation from the averaging approximation Eq. (16) of the Winfree model for AS, RP, and square pulses with $\Pi = 10/11$—see Table I. Panels (a), (b), and (c) correspond to $q = -1$, $q = 0$, and $q = 1$, respectively. The inset in panel (b) shows the curves in log-log scale. The thick solid line has slope 2 and is plotted as a guide for the eye.

detailed investigation of its collective dynamics. In Ref. [50], we considered the pulse type originally adopted by Ariaratnam and Strogatz in Ref. [15] and then used in numerous studies [42–45,48–50,54].

Here we have additionally investigated the Winfree model with rectified Poisson and square pulses. For these pulse types the numerical study of the system of two ODEs in Eq. (11) is simpler because, in contrast to the AS pulse, their associated mean-field functions $h(Z)$ do not become increasingly convoluted as the pulse width is decreased (see Table I). Indeed, the numerical investigation of Eq. (11) for very narrow AS pulses is impracticable, but not for RP and Square pulses.

Another question is that AS and RP pulses are nonvanishing in $\theta \in (-\pi,\pi)$. This means that a pulse is emitted during the entire period of rotation of an oscillator (or even when the oscillator becomes quiescent). In some cases this interaction type may be unrealistic. For example, neuronal interactions may be mediated by action potentials, which are brief, all-or-none events that are better modeled using narrow squarelike pulses.

Regarding the PRCs, we considered sinusoidally shaped PRCs with positive, negative, and zero offsets q. The case of negative offset was not considered in Ref. [50] but has been revealed to be interesting and nontrivial. Indeed, the claim that narrow pulses are optimal for synchronizing large populations of oscillators [50] does not hold for negative PRC offsets. In this case, we find that the optimal pulse, allowing to synchronize more heterogeneous populations, has an intermediate width; see Fig. 6(a). Moreover, PRCs with a negative offset are more likely to have a synchronization scenario with five codimension-two points (including BT′), in contrast to the scenario with three already reported in Ref. [50]—see Fig. 4. The conditions under which each of the scenarios is found depend on the particular pulse type. From our results, we inferred that pulses that are closer to zero at phases far from the peak phase are more likely to exhibit a BT′ point. In fact, the RP pulse does not exhibit a BT′ point for any q value, while the square pulse already does for a balanced PRC ($q = 0$). We also considered the limit of infinitely narrow pulses (Dirac δ pulses) and provided exact formulas for the synchronization boundary (a Hopf bifurcation). Additionally, we demonstrated that positive PRC offsets display larger synchronization regions and are capable of synchronizing more heterogeneous ensembles. It would be interesting to investigate whether there exists some natural system where the intrinsic PRCs and the pulse shape/type is correlated in a way consistent with these results.

Finally, we have compared the synchronization threshold of the Winfree model with its averaging approximation (the Kuramoto-Sakaguchi model). The results indicate that the predictions of averaging are more inaccurate as $|q|$ grows, changing in opposite directions depending of the sign of q.

In future studies, it would be interesting to find techniques to efficiently analyze the Winfree model with nonsinusoidal PRC, as well as for frequency distributions other than the Lorentzian one. The study in Ref. [15] for a uniform distribution of natural frequencies is valuable, but it is difficult to extend it to nonvanishing q. On the other hand, Eq. (14) permits us to use the mean field Eq. (11) with other pulse types and to investigate, for example, the impact of asymmetric, or multimodal pulses on collective synchronization. Generalizing the model by considering other sources of heterogeneity is also an interesting venue for future research.

ACKNOWLEDGMENTS

We acknowledge support by MINECO (Spain) under Projects No. FIS2014-59462-P, No. FIS2016-74957-P, No. PSI2016-75688-P, and No. PCIN-2015-127. E.M. and D.P. also acknowledge support by the European Union's Horizon 2020 research and innovation programme under the Marie Skłodowska-Curie Grant Agreement No. 642563.

[1] A. T. Winfree, On emerging coherence, Science **298**, 2336 (2002).
[2] S. H. Strogatz, From Kuramoto to Crawford: Exploring the onset of synchronization in populations of coupled oscillators, Physica D **143**, 1 (2000).
[3] A. S. Pikovsky, M. G. Rosenblum, and J. Kurths, *Synchronization, a Universal Concept in Nonlinear Sciences* (Cambridge University Press, Cambridge, 2001).
[4] S. H. Strogatz, *Sync: The Emerging Science of Spontaneous Order* (Hyperion Press, New York, 2003).
[5] J. Buck and E. Buck, Synchronous fireflies, Sci. Am. **234**, 74 (1976).
[6] C. Liu, D. R. Weaver, S. H. Strogatz, and S. M. Reppert, Cellular construction of a circadian clock: Period determination in the suprachiasmatic nuclei, Cell **91**, 855 (1997).
[7] L. Glass and M. C. Mackey, *From Clocks to Chaos: The Rhythms of Life* (Princeton University Press, Princeton, NJ, 1988).
[8] S. H. Strogatz, B. Eckhardt, D. M. Abrams, A. McRobie, and E. Ott, Theoretical mechanics: Crowd synchrony on the Millennium bridge, Nature **438**, 43 (2005).
[9] Z. Néda, E. Ravasz, Y. Brechet, T. Vicsek, and A.-L. Barabási, Self-organizing processes: The sound of many hands clapping, Nature **403**, 849 (2000).
[10] I. Kiss, Y. Zhai, and J. L. Hudson, Emerging coherence in population of chemical oscillators, Science **296**, 1676 (2002).
[11] G. Heinrich, M. Ludwig, J. Qian, B. Kubala, and F. Marquardt, Collective Dynamics in Optomechanical Arrays, Phys. Rev. Lett. **107**, 043603 (2011).
[12] K. Wiesenfeld, P. Colet, and S. H. Strogatz, Synchronization Transitions in A Disordered Josephson Series Array, Phys. Rev. Lett. **76**, 404 (1996).
[13] A. T. Winfree, Biological rhythms and the behavior of populations of coupled oscillators, J. Theor. Biol. **16**, 15 (1967).
[14] A. T. Winfree, *The Geometry of Biological Time* (Springer, New York, 1980).
[15] J. T. Ariaratnam and S. H. Strogatz, Phase Diagram for the Winfree Model of Coupled Nonlinear Oscillators, Phys. Rev. Lett. **86**, 4278 (2001).
[16] D. D. Quinn, R. H. Rand, and S. H. Strogatz, Singular unlocking transition in the Winfree model of coupled oscillators, Phys. Rev. E **75**, 036218 (2007).
[17] L. Basnarkov and V. Urumov, Critical exponents of the transition from incoherence to partial oscillation death in the Winfree model, J. Stat. Mech. (2009) P10014.
[18] J. A. Acebrón, L. L. Bonilla, C. J. Pérez-Vicente, F. Ritort, and R. Spigler, The Kuramoto model: A simple paradigm for synchronization phenomena, Rev. Mod. Phys. **77**, 137 (2005).
[19] E. Ott and T. M. Antonsen, Low dimensional behavior of large systems of globally coupled oscillators, Chaos **18**, 037113 (2008).
[20] E. Ott and T. M. Antonsen, Long time evolution of phase oscillator systems, Chaos **19**, 023117 (2009).
[21] E. Ott, B. R. Hunt, and T. M. Antonsen, Comment on "long time evolution of phase oscillators systems," Chaos **21**, 025112 (2011).
[22] T. M. Antonsen, Jr., R. T. Faghih, M. Girvan, E. Ott, and J. Platig, External periodic driving of large systems of globally coupled phase oscillators, Chaos **18**, 037112 (2008).
[23] A. Pikovsky and M. Rosenblum, Partially Integrable Dynamics of Hierarchical Populations of Coupled Oscillators, Phys. Rev. Lett. **101**, 264103 (2008).
[24] L. M. Childs and S. H. Strogatz, Stability diagram for the forced Kuramoto model, Chaos **18**, 043128 (2008).
[25] D. M. Abrams, R. Mirollo, S. H. Strogatz, and D. A. Wiley, Solvable Model for Chimera States of Coupled Oscillators, Phys. Rev. Lett. **101**, 084103 (2008).
[26] M. M. Abdulrehem and E. Ott, Low dimensional description of pedestrian-induced oscillation of the millenium bridge, Chaos **19**, 013129 (2009).
[27] D. Pazó and E. Montbrió, Existence of hysteresis in the Kuramoto model with bimodal frequency distributions, Phys. Rev. E **80**, 046215 (2009).
[28] E. A. Martens, E. Barreto, S. H. Strogatz, E. Ott, P. So, and T. M. Antonsen, Exact results for the Kuramoto model with a bimodal frequency distribution, Phys. Rev. E **79**, 026204 (2009).
[29] W. S. Lee, E. Ott, and T. M. Antonsen, Large Coupled Oscillator Systems with Heterogeneous Interaction Delays, Phys. Rev. Lett. **103**, 044101 (2009).
[30] L. F. Lafuerza, P. Colet, and R. Toral, Nonuniversal Results Induced by Diversity Distribution in Coupled Excitable Systems, Phys. Rev. Lett. **105**, 084101 (2010).
[31] L. M. Alonso and G. B. Mindlin, Average dynamics of a driven set of globally coupled excitable units, Chaos **21**, 023102 (2011).
[32] H. Hong and S. H. Strogatz, Kuramoto Model of Coupled Oscillators with Positive and Negative Coupling Parameters: An Example of Conformist and Contrarian Oscillators, Phys. Rev. Lett. **106**, 054102 (2011).
[33] E. Montbrió and D. Pazó, Shear Diversity Prevents Collective Synchronization, Phys. Rev. Lett. **106**, 254101 (2011).
[34] G. Barlev, T. M. Antonsen, and E. Ott, The dynamics of network coupled phase oscillators: An ensemble approach, Chaos **21**, 025103 (2011).
[35] A. Pikovsky and M. Rosenblum, Dynamics of heterogeneous oscillator ensembles in terms of collective variables, Physica D **240**, 872 (2011).
[36] O. E. Omel'chenko and M. Wolfrum, Nonuniversal Transitions to Synchrony in the Sakaguchi-Kuramoto Model, Phys. Rev. Lett. **109**, 164101 (2012).
[37] S. Petkoski and A. Stefanovska, Kuramoto model with time-varying parameters, Phys. Rev. E **86**, 046212 (2012).
[38] D. Iatsenko, S. Petkoski, P. V. E. McClintock, and A. Stefanovska, Stationary and Traveling Wave States of the Kuramoto Model with An Arbitrary Distribution of Frequencies and Coupling Strengths, Phys. Rev. Lett. **110**, 064101 (2013).
[39] J. G. Restrepo and E. Ott, Mean-field theory of assortative networks of phase oscillators, Europhys. Lett. **107**, 60006 (2014).
[40] B. Pietras, N. Deschle, and A. Daffertshofer, Equivalence of coupled networks and networks with multimodal frequency distributions: Conditions for the bimodal and trimodal case, Phys. Rev. E **94**, 052211 (2016).
[41] E. Ott and T. M. Antonsen, Jr., Frequency and phase synchronization in large groups: Low-dimensional description of synchronized clapping, firefly flashing, and cricket chirping, Chaos **27**, 051101 (2017).

[42] T. B. Luke, E. Barreto, and P. So, Complete classification of the macroscopic behavior of a heterogeneous network of theta neurons, Neural Comput. **25**, 3207 (2013).

[43] P. So, T. B. Luke, and E. Barreto, Networks of theta neurons with time-varying excitability: Macroscopic chaos, multistability, and final-state uncertainty, Physica D **267**, 16 (2014).

[44] C. R. Laing, Derivation of a neural field model from a network of theta neurons, Phys. Rev. E **90**, 010901 (2014).

[45] C. R. Laing, Exact neural fields incorporating gap junctions, SIAM J. Appl. Dyn. Syst. **14**, 1899 (2015).

[46] E. Montbrió, D. Pazó, and A. Roxin, Macroscopic Description for Networks of Spiking Neurons, Phys. Rev. X **5**, 021028 (2015).

[47] D. Pazó and E. Montbrió, From Quasiperiodic Partial Synchronization to Collective Chaos in Populations of Inhibitory Neurons with Delay, Phys. Rev. Lett. **116**, 238101 (2016).

[48] K. P. O'Keeffe and S. H. Strogatz, Dynamics of a population of oscillatory and excitable elements, Phys. Rev. E **93**, 062203 (2016).

[49] S. Chandra, D. Hathcock, K. Crain, T. M. Antonsen, M. Girvan, and E. Ott, Modeling the network dynamics of pulse-coupled neurons, Chaos **27**, 033102 (2017).

[50] D. Pazó and E. Montbrió, Low-Dimensional Dynamics of Populations of Pulse-Coupled Oscillators, Phys. Rev. X **4**, 011009 (2014).

[51] A. J. Preyer and R. J. Butera, Neuronal Oscillators in Aplysia Californica that Demonstrate Weak Coupling *in Vitro*, Phys. Rev. Lett. **95**, 138103 (2005).

[52] T. Tateno and H. P. C. Robinson, Phase resetting curves and oscillatory stability in interneurons of rat somatosensory cortex, Biophys. J. **92**, 683 (2007).

[53] B. Kralemann, M. Frühwirth, A. Pikovsky, M. Rosenblum, T. Kenner, J. Schaefer, and M. Moser, *In vivo* cardiac phase response curve elucidates human respiratory heart rate variability, Nat. Commun. **4**, 2418 (2013).

[54] P. Goel and B. Ermentrout, Synchrony, stability, and firing patterns in pulse-coupled oscillators, Physica D **163**, 191 (2002).

[55] For the finite-N system, the asymptotic dynamics of the Winfree model appears to be consistent with the OA theory for the discretization of $g(\omega)$ we adopted, consisting of one oscillator per frequency value. Indeed some theoretical progress confirming the usefulness of the OA ansatz to characterize the dynamics of finite populations has been recently achieved [67].

[56] B. Pietras and A. Daffertshofer, Ott-Antonsen attractiveness for parameter-dependent oscillatory systems, Chaos **26**, 103101 (2016).

[57] Actually, in Refs. [20,21] this result is shown for Eq. (6) with $B(t) = 0$, which can always be achieved by the change of variables $\theta_i' = \theta_i - b(t)$ where $\dot{b}(t) = B(t)$ [50].

[58] R. E. Mirollo, The asymptotic behavior of the order parameter for the infinite-N Kuramoto model, Chaos **22**, 043118 (2012).

[59] W. H. Press, S. A. Teukolsky, W. T. Vetterling, and B. P. Flannery, *Numerical Recipes in FORTRAN: The Art of Scientific Computing*, 2nd ed. (Cambridge University Press, New York, NY, 1992), Chap. 16.

[60] S. Shinomoto and Y. Kuramoto, Phase transitions in active rotator systems, Prog. Theor. Phys. **75**, 1105 (1986).

[61] J. Guckenheimer and P. Holmes, *Nonlinear Oscillations, Dynamical Systems, and Bifurcations of Vector Fields* (Springer-Verlag, New York, 1983).

[62] Y. A. Kuznetsov, *Elements of Applied Bifurcation Theory* (Springer Verlag, New York, 1998).

[63] R. Zillmer, R. Livi, A. Politi, and A. Torcini, Stability of the splay state in pulse-coupled networks, Phys. Rev. E **76**, 046102 (2007).

[64] Y. Kuramoto, *Chemical Oscillations, Waves, and Turbulence* (Springer-Verlag, Berlin, 1984).

[65] H. Sakaguchi and Y. Kuramoto, A soluble active rotator model showing phase transitions via mutual entrainment, Prog. Theor. Phys. **76**, 576 (1986).

[66] O. E. Omel'chenko and M. Wolfrum, Is there an impact of small phase lags in the Kuramoto model? Chaos **26**, 094806 (2016).

[67] V. Vlasov, M. Rosenblum, and A. Pikovsky, Dynamics of weakly inhomogeneous oscillator populations: Perturbation theory on top of Watanabe-Strogatz integrability, J. Phys. A: Math. Theor. **49**, 31LT02 (2016).